

Evolution of sandstone shear strength parameters and its mesoscopic mechanism

Hao Shi^{1,2}, Houquan Zhang*¹ and Lei Song¹

¹State Key Laboratory for Geomechanics & Deep Underground Engineering, School of Mechanics & Civil Engineering, China University of Mining and Technology, Xuzhou, 221116, People's Republic of China

²GeoEnergy Research Centre, University of Nottingham, Nottingham NG7 2RD, U.K

(Received November 25, 2019, Revised December 23, 2019, Accepted December 26, 2019)

Abstract. It is extremely important to obtain rock strength parameters for geological engineering. In this paper, the evolution of sandstone cohesion and internal friction angle with plastic shear strain was obtained by simulating the cyclic loading and unloading tests under different confining pressures using Particle Flow Code software. By which and combined with the micro-crack propagation process, the mesoscopic mechanism of parameter evolution was studied. The results show that with the increase of plastic shear strain, the sandstone cohesion decreases first and then tends to be stable, while the internal friction angle increases first, then decreases, and finally maintains unchanged. The evolution of sandstone shear strength parameters is closely related to the whole process of crack formation, propagation and coalescence. When the internal micro-cracks are less and distributed randomly and dispersedly, and the rock shear strength parameters (cohesion, internal friction angle) are considered to have not been fully mobilized. As the directional development of the internal micro-fractures as well as the gradual formation of macroscopic shear plane, the rock cohesion reduces continuously and the internal friction angle is in the rise stage. As the formation of the macroscopic shear plane, both the rock cohesion and internal friction angle continuously decrease to a certain residual level.

Keywords: strength parameter evolution; plastic shear strain; mesoscopic mechanism; numerical study; sandstone

1. Introduction

For the slope engineering, it is a gradual-developed process for the slip along the slip surface. That the internal load exceeds the bearing capacity of the rock will raise the generation of plastic strain and the attenuation of mechanical parameters (such as cohesion, internal friction angle) at the local position (Langford and Diederichs 2015, Shi *et al.* 2019a, Wang *et al.* 2017). So that the stress will be redistributed accordingly, which will be further affected the adjacent area. As a result, the plastic area will gradually expand, eventually leading to overall instability of the slope along the slip surface (see Fig. 1). Therefore, it is of great significance to ensure the slope stability by in-depth study of the rock damage evolution, mastering the internal relationship between rock deformation and strength parameters, and then choosing a correct support method (Shi *et al.* 2019b, Renani and Martin 2018).

After reaching the peak strength, the axial stress of rock specimen will gradually decrease with the axial strain until that the residual strength is reached. This rock strength degradation phenomenon driven by deformation is called 'strain softening' (Hajiabdolmajid *et al.* 2003, Zhang *et al.* 2008). The traditional strain softening model is not complete enough to describe the variation of rock strength



Fig. 1 Instability slip of Daping slope in Fengjie County, Chongqing City, China

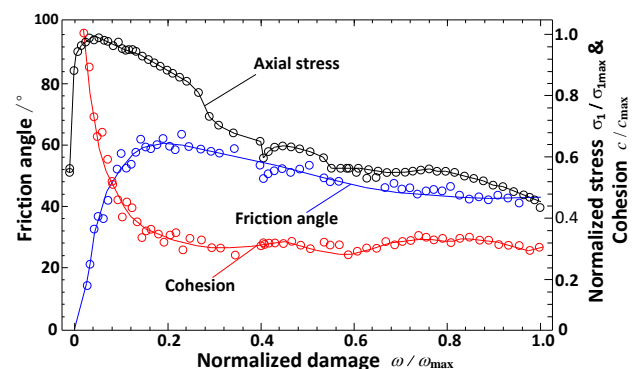


Fig. 2 Evolution of rock cohesion and internal friction angle with damage (Martin and Chandler 1994)

*Corresponding author, Associate Professor
E-mail: zhanghouquan_cumt@163.com

parameters adopting the peak strain as the zero point of the plastic parameter (Carpenter *et al.* 2011, Haerberli *et al.* 2010, Martin and Chandler 1994), due to the fact that significant plastic deformation of rock is produced in the pre-peak stage, as the measured results shown in Fig. 2. The study of variation of rock strength parameters in the pre-peak yield hardening and post-peak strain softening stages, to make up for the shortcomings of the traditional strain softening model, has been a hot topic for scholars in the field of geotechnical engineering as well as of abundant results already achieved.

The relationship between rock strength parameters and damage variable was established based on the Mohr-Coulomb (M-C) strength criterion and uniaxial cyclic loading and unloading experiments on granite (Martin and Chandler 1994, Renani and Martin 2018). Which can be described as that the rock cohesion and the internal friction angle are synchronously mobilized, and with the increase of the normalized damage, the internal friction angle increases first, then decreases, and finally stabilizes, while the cohesion first decreases rapidly and then tends to be stable, as can be seen in Fig. 2.

On the basis of the M-C strength criterion and using different research methods, the researchers (Hajiabdolmajid *et al.* 2003, Joseph 2000, Zhang *et al.* 2008) obtained different evolution models of the strength parameter for different rock categories, including the cohesion weakening-frictional strengthening model (CWFS) (Hajiabdolmajid *et al.* 2003), the nonlinear CWFS model (Renani and Martin 2018), the cohesion softening-friction hardening model (CSFH) (Edelbro 2010) and cohesion softening-friction unchanging model (CSFU) (Zhang *et al.* 2008). The above researches are of great significance for understanding the process of rock damage. However, for the evolution of rock strength parameters, most researchers do not give an explanation, and the rare explanations are of lacking evidence.

In this paper, the cyclic loading and unloading experiments of sandstone under different confining pressures was simulated using PFC^{2D}, then the plastic shear strain picked from the curves is taken as an internal variable to obtain the evolution of rock cohesion and internal friction angle on the basis of M-C strength criterion. Afterwards, the mesoscopic mechanism of the parameter evolution was studied in combination with the micro crack propagation process. Finally, a comparative study of FLAC^{2D} (Fast Lagrangian Analysis of Continua) simulation was carried out to verify the reliability of the obtained evolution of sandstone cohesion and internal friction angle.

2. Particle flow-based numerical simulation of sandstone cycle loading and unloading test

To study the evolution process of sandstone strength parameters (cohesion, internal friction angle) with plastic strain, it is necessary to accurately obtain the corresponding plastic strain of specimen at different stress points, and the effective means to achieve which is rock cyclic loading and unloading test. As this paper intends to explain the mesoscopic mechanism of the evolution process of rock

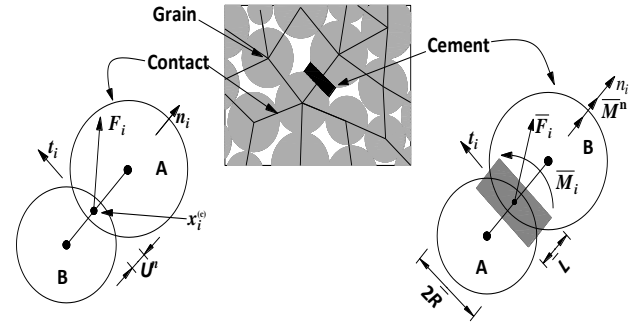


Fig. 3 Two kinds of bond form in BPM (Potyondy *et al.* 2004)

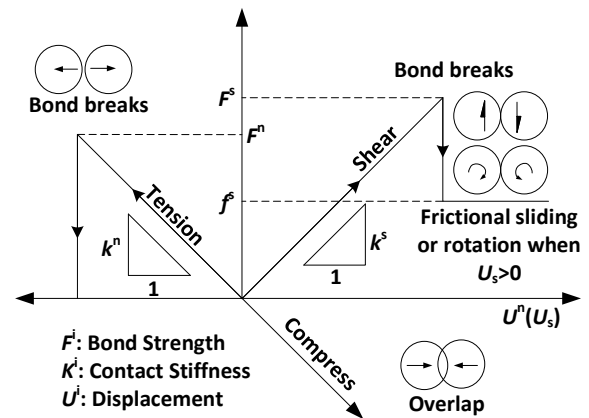


Fig. 4 Force-displacement relationships between particles in BPM (Potyondy *et al.* 2004)

strength parameters, but it is difficult to obtain rock crack propagation information through laboratory experiments (especially for triaxial compression tests). Therefore, numerical simulation of rock cyclic loading and unloading test by PFC^{2D} software, as a novel method to reveal the mesoscopic mechanism of strength parameter evolution, is carried out in this article.

2.1 PFC^{2D} simulation principle of sandstone particle bond and internal friction

PFC^{2D}, the commercial discrete element software developed by Itasca company, is applied to simulate the cohesion and friction behaviors between rock mineral particles by characterizing a collection of rigid particles as the medium. Without complicated constitutive model and flow criterion in PFC^{2D} software, the complex mechanical behaviors of the macroscopic model are realized by the change of particle contact state, which is described by the equation of motion (used to characterize the particle state), the simple mechanical constitutive relation (used to characterize force-displacement / rotation relationship between particles) and the yield criterion (used to identify whether or not the bond failure occurs and the type of failure) (Shan and Lai 2019). The bonded-particle model (BPM) (Potyondy *et al.* 2004), as the combination of the contact bond and parallel bond built in PFC^{2D} software, is adopted to simulate in this paper.

Circular particles are used (see Fig. 3) as discrete

elements in the BPM model of this article, and the force relationship between the particles is divided into two parts, one is the contact force generated by the contact of the particles (after overlapping) and the other is the force and moment generated by the parallel bond.

For contact bond, the interaction force between particles (A and B) can be decomposed along the normal and tangential directions of the contact surface as follows,

$$F_i = F^n n_i + F^s t_i \quad (1)$$

where, F^n and F^s are respectively called the normal contact force and the tangential contact force; n_i and t_i are unit normal vector and the tangential vector along the contact surface, correspondingly. In addition, the tangential contact force F^s between the particles cannot exceed the product of the normal contact force and the friction coefficient, as follows,

$$F^s \leq \zeta F^n \quad (2)$$

where ζ is taken as the minimum value of the friction coefficients of particles A and B.

It should be noted that contact bond, the most basic mode of interaction between the particles, cannot reflect the moment between the particles. While the parallel bond can be seen as a set of springs distributed in a rectangular area centered on the contact point, by which both the force and the moment can be transmitted (Potyondy *et al.* 2004), as shown in Fig. 3.

The force-displacement relationship of the parallel bond is described by the following five parameters: normal stiffness, \bar{k}^n , tangential stiffness, \bar{k}^s , tensile strength, $\bar{\sigma}_c$, shear strength, $\bar{\tau}_c$, and bond-radius multiplier, $\bar{\lambda}$.

Parallel bond radius can be calculated by the following formula,

$$\bar{R} = \bar{\lambda} \min(R^{(A)}, R^{(B)}) \quad (3)$$

with $R^{(A)}$ and $R^{(B)}$ being the radii of particles A and B, respectively.

The elastic force and moment are expressed in increment form as follows,

$$\begin{cases} \Delta \bar{F}^n = \bar{k}^n A \Delta U^n \\ \Delta \bar{F}^s = -\bar{k}^s A \Delta U^s \\ \Delta \bar{M}^n = -\bar{k}^n J \Delta \theta^n \\ \Delta \bar{M}^s = -\bar{k}^s J \Delta \theta^s \end{cases} \quad (4)$$

where A , I , and J represent the area, the inertia moment, and the polar moment of inertia of the parallel bond, respectively. ΔU^n , ΔU^s and $\Delta \theta^n$, $\Delta \theta^s$ are increments of relative displacements and angular in the normal and tangential directions (Potyondy *et al.* 2004).

The maximum tensile stress and shear stress applied on the parallel bond is satisfied the following formula,

$$\begin{cases} \bar{\sigma}^{\max} = \frac{-\bar{F}^n}{A} + \frac{|\bar{M}^s| \bar{R}}{I} < \bar{\sigma}_c \\ \bar{\tau}^{\max} = \frac{|\bar{F}^s|}{A} + \frac{|\bar{M}^n| \bar{R}}{J} < \bar{\tau}_c \end{cases} \quad (5)$$

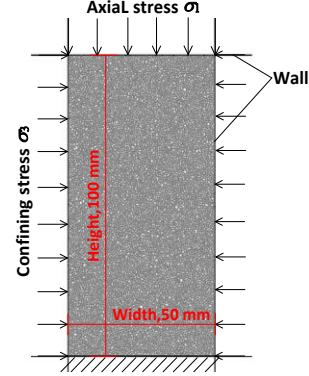


Fig. 5 Geometric calculation model

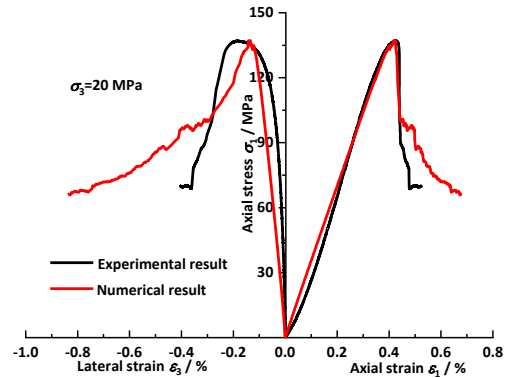


Fig. 6 The comparison of simulation and experimental stress-strain curves of sandstone specimen

with $\bar{\sigma}_c$ and $\bar{\tau}_c$ being the tensile strength and shear strength. When the tensile stress is greater than the tensile strength, the tensile strength will be reduced to 0 with tensile cracks generated. Similarly, when the shear stress is greater than the shear strength, the shear strength will be reduced to a certain residual value and the shear tensile cracks will be generated. The force-displacement relationships (Potyondy *et al.* 2004) of tension, compression and shear between particles are shown in Fig. 4.

According to the above description, both the contact bond and parallel bond should exist inside the rock, which is why that the BPM is adopted in this paper.

2.2 Establishment of geometric model and boundary constraints

As shown in Fig. 5, the two-dimensional planar model with a size of 50 mm \times 100 mm and containing approximately 20,000 ball units is used in this article, and the four rigid walls of the geometric model are imposed boundary constraints: a displacement constraint is applied to the bottom, a confining pressure is applied laterally and loading stress is applied at the top.

2.3 Calibration of sandstone mesoscopic parameters

It is obvious that the axial strain of the three-dimensional actual specimen can be characterized by the axial strain of the two-dimensional planar model. For its circumferential strain, it can be expressed by the following

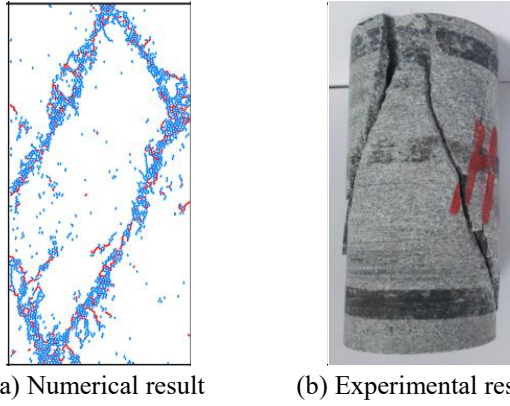


Fig. 7 Failure modes of sandstone specimens obtained through simulation and experiment

Table 1 Rock microscopic physical and mechanical properties of BPM

Parameters	Value
Minimum particle size R_{\min} /mm	0.2
Maximum particle size R_{\max} /mm	0.6
Density ρ /($\text{kg}\cdot\text{m}^{-3}$)	2700
Porosity n /%	1.5
Friction coefficient μ	0.8
Particle stiffness ratio r_b	3
Contact-bond modulus E_b /GPa	5
Contact-bond stiffness ratio r	2
Parallel-bond tensile strength $\bar{\sigma}_t$ /MPa	5.5
Parallel-bond shear strength $\bar{\tau}_c$ /MPa	17.5
Parallel-bond modulus \bar{E} /GPa	15
Parallel-bond radius factor $\bar{\lambda}$	1.4

formula,

$$\varepsilon_3^{3D} = \frac{2\pi r' - 2\pi r}{2\pi r} = \frac{2r' - 2r}{2r} = \varepsilon_3^{2D} \quad (6)$$

where r' and r respectively represent the radii of the specimen under the load and the original radius; ε_3^{3D} and ε_3^{2D} represent the three-dimensional circumferential strain and the two-dimensional lateral strain, respectively. As can be seen from the Eq. 6, the three-dimensional lateral strain can also be characterized by the two-dimensional lateral strain.

The sandstone strength mesoscopic parameters are calibrated by the “trial and error” method (Castro-Filgueira *et al.* 2017, Wang and Tian 2018) according to the full stress-strain test curve and failure mode of sandstone under the confining stress of 20 MPa. The main calibration process can be described as that, (1) Adjust the contact modulus to obtain the same elastic modulus as the experimental specimen; (2) Adjust the cohesive strength and tensile strength of the parallel bond to obtain the same peak stress as the corresponding experimental curve; (3) Fine-tune the parameters to obtain the failure mode similar to the experimental specimen. The stress-strain curve (see Fig. 6) and the final failure characteristics (see Fig. 7) of

PFC^{2D} model under 20 MPa confining pressure are in good agreement with the laboratory result of sandstone. The model parameters calibrated by “trial and error” method are shown in Table 1.

2.4 Simulation results of sandstone cycle loading and unloading test

For the simulation of cyclic loading and unloading tests, the confining pressures are 3.5 MPa, 5 MPa, 10 MPa, 15 MPa and 20 MPa, respectively; the loading process is controlled by displacement, while the unloading is controlled by stress. During the loading process, the upper wall is continuously moved downward with a speed of 0.002 mm/s until the strain reaches the preset value, then the unloading process with the confining pressure maintained is carried out with the speed of -0.001 mm/s until that the axial stress is less than 1 Pa. During the test process, the software can automatically record the parameters such as stress, strain and the number of micro-cracks as well as show the extended state of micro-cracks in real time. In addition, there are two main conditions for controlling the number of cycles, one is that all the samples must be loaded to the residual stress stage; the other is that the final plastic shear strain of the sample under each confining pressure, as the sum of axial strain and lateral strain, should be approximately equal.

The sandstone cycle loading and unloading simulation results are shown in Fig. 8. According to the simulation results, the following conclusions can be obtained, (1) In the elastic phase of the pre-peak stage, the unloading curve is basically coincided with the reloading curve, and when the specimen is nonlinearly deformed, a hysteresis effect begins to occur between the unloading curve and the reloading curve (Li *et al.* 2017). (2) The starting point of plastic deformation is closer to the linear-nonlinear turning point of the stress-strain curve, that is, plastic deformation has been already occurred at the pre-peak stage. What's more, the growth rate of lateral plastic strain is significantly greater than that of axial plastic strain. (3) According to the stress-strain curves, the elastic moduli of specimens under different confining pressures are all close to 32 GPa, while the Poisson's ratio decreases with the increase of confining pressure. Specifically, the Poisson's ratios of the specimens under the confining pressures of 3.5 MPa, 5 MPa, 10 MPa, 15 MPa and 20 MPa are 0.375, 0.346, 0.310, 0.294 and 0.289, respectively. (4) Both the peak strength σ_p and residual strength σ_r of the specimens increase linearly with the increase of confining pressure, as shown in Fig. 9.

3. Evolution model of sandstone strength parameters

3.1 Strain-softening model based on M-C criterion

The expression of the M-C criterion is as follows,

$$\left. \begin{aligned} f^s &= \sigma_1 - \sigma_3 N_\varphi + 2c\sqrt{N_\varphi} \\ N_\varphi &= (1 + \sin \varphi) / (1 - \sin \varphi) \end{aligned} \right\} \quad (7)$$

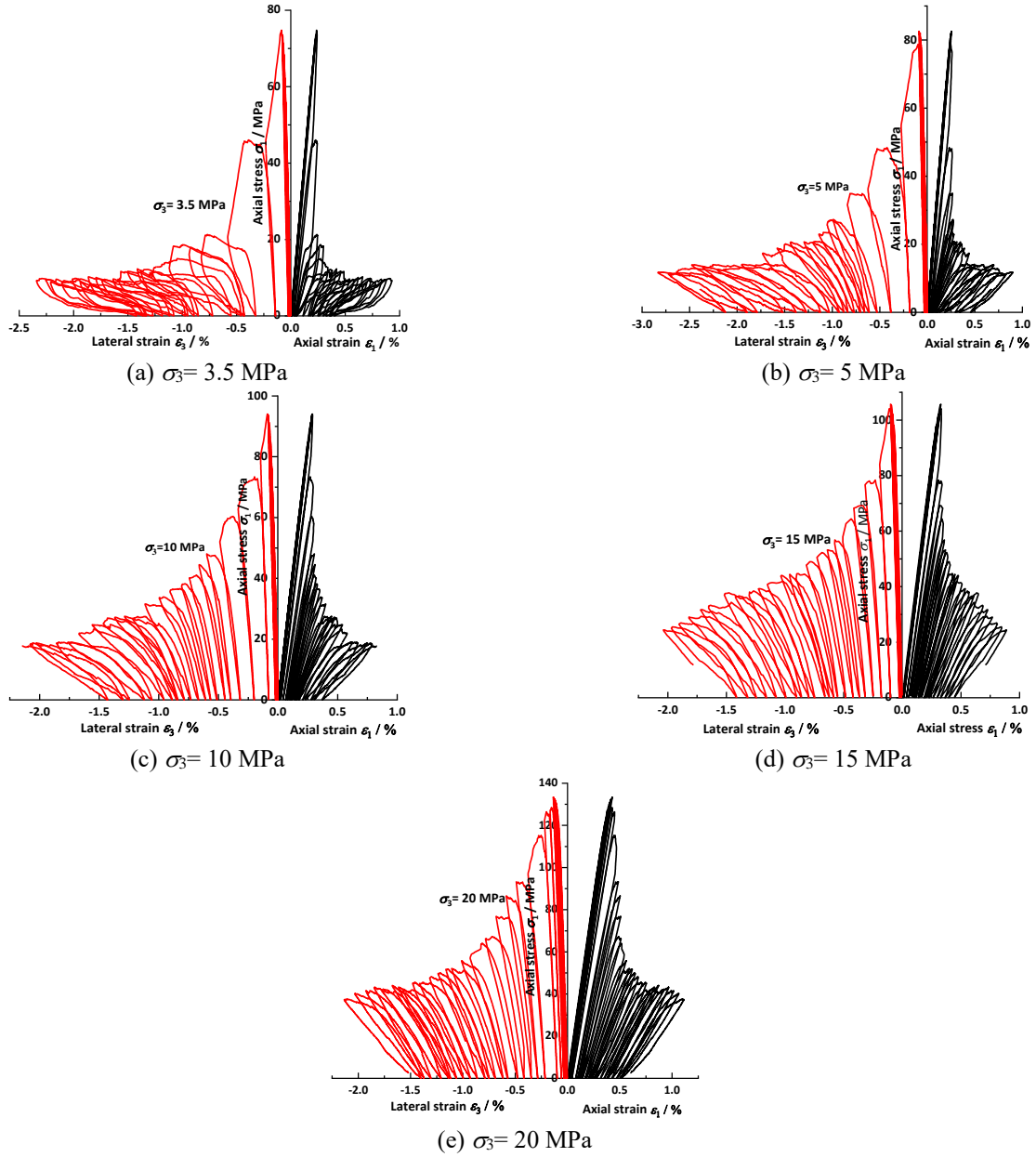


Fig. 8 Full stress-strain curves of sandstone specimens under different confining pressures

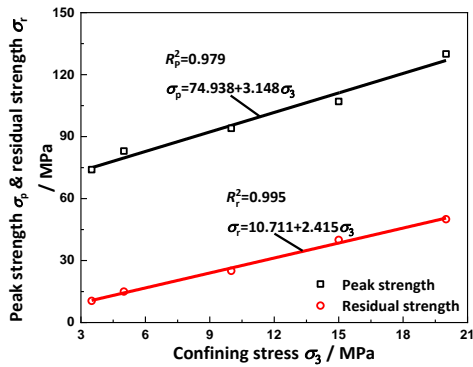


Fig. 9 Relationship between peak σ_p / residual strength σ_r and confining pressures σ_3

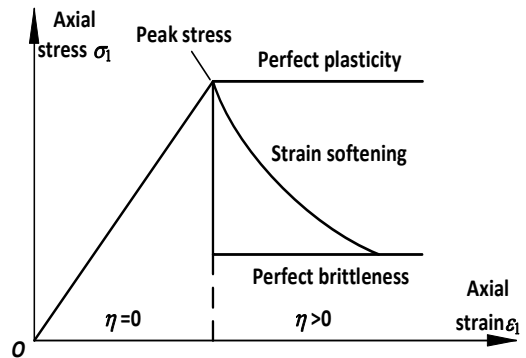


Fig. 10 Post-peak softening model and its special cases

That $f^s < 0$ indicates that the specimen is still in the elastic stage or has not been reached its bearing limit; That $f^s = 0$

indicates that the test piece is in the yield state and the rock deformation is mainly plastic. The corresponding plastic flow law is as follows,

$$\Delta \varepsilon_i^{ps} = \lambda^s \frac{\partial g^s}{\partial \sigma_i} \quad (8)$$

where $\Delta \varepsilon_i^{ps}$ ($i=1,3$) is the incremental form of the principal plastic strain component, λ^s is the plastic multiplication factor, g^s is the plastic potential function and σ_i ($i=1,3$) is the principal stress component.

The above is a brief introduction to the M-C strength criterion. The strain softening model, a widely used model under M-C criterion system, can be expressed more abundant stress paths of rock post-peak stage compared with the ideal brittleness and ideal plasticity model, as shown in Fig. 10. In order to describe the deterioration of the rock strength, which is related to the cohesion and the internal friction angle (see Fig. 2), a parameter needs to be introduced to change (degrade) the cohesion and internal friction angle according to a certain law. Therefore, compared with the M-C strength criterion, a plasticity parameter η is introduced into the strain-softening model, thus the yield function of the model can be changed to expressed as follows,

$$f^s(\sigma_{ij}, \eta, c_\eta, \varphi_\eta) = 0 \quad (9)$$

where σ_{ij} is the principal stress tensor, c_η and φ_η are the cohesion and the internal friction angle changed with the plastic parameter η . This formula is adopted to express a constraint relationship between rock stress (strength) tensor, cohesion, internal friction angle and plasticity parameters during the yielding phase.

The peak strain is often used as the starting point of the plastic parameter evolution for the traditional strain-softening model, as shown in Fig. 10. But in fact, significant plastic deformation has been produced in the pre-peak stage, as shown in Fig. 8. Which shows that the traditional strain softening model is not complete enough to describe the variation of rock strength parameters. Hence it is necessary to correct and perfect the traditional model.

3.2 Selection of plastic parameter

In the strain softening model, there are many kinds of plastic parameters commonly adopted to describe the variation of rock strength parameters, such as plastic work, plastic volume strain and plastic shear strain. The selection of plastic parameter is very important, and the ideal plastic parameter needs to be with the three characteristics of cumulativity, uniqueness and spatiality (Li *et al.* 2017, Wu *et al.* 2018a). In addition, the form of the selected parameter should be as concise as possible. Thus, plastic shear strain (in two dimension), a parameter that more closely conforms to the characteristics of ideal plastic parameters, is used as the plasticity parameter in this paper, which can be obtained by the following formula,

$$\gamma_p = \varepsilon_1^{ps} - \varepsilon_3^{ps} \quad (10)$$

with ε_1^{ps} and ε_3^{ps} being the maximum and minimum principal plastic strains, respectively, and γ_p being the two-dimensional plastic shear strain. To keep consistent with the abscissa of the curves in Fig. 8, the axial compression

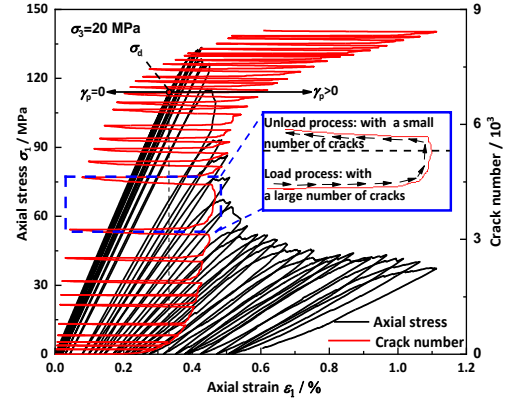


Fig. 11 Full stress-strain curve and crack number of sandstone specimen

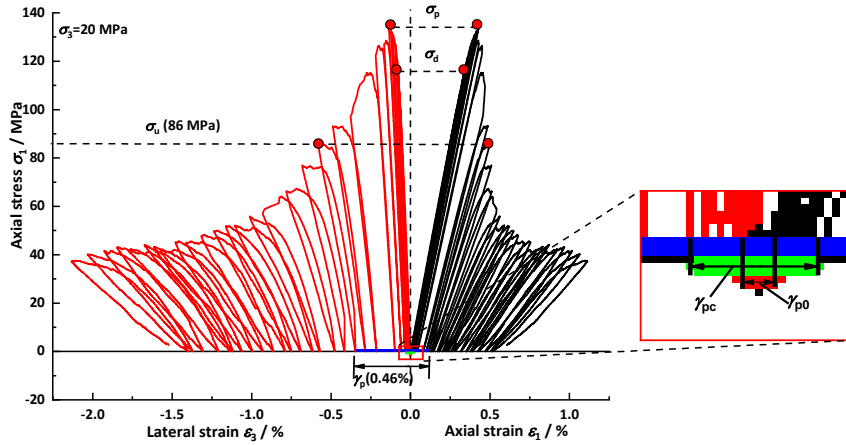
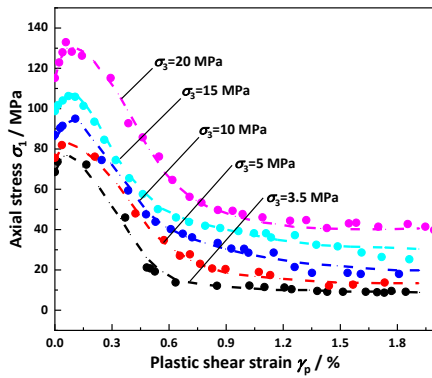
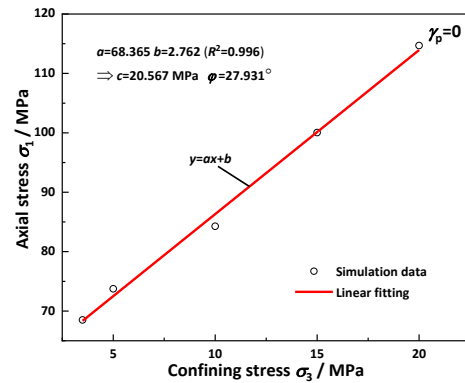
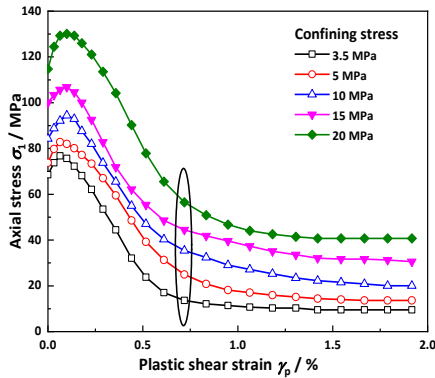
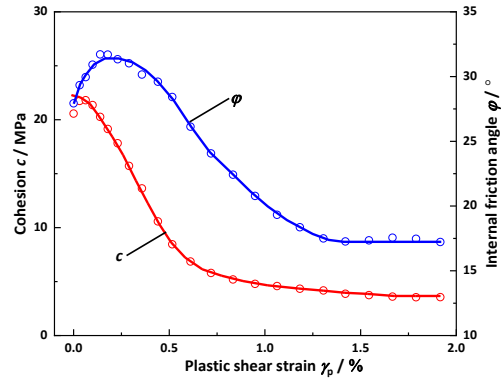
deformation and the lateral expansion deformation are set to be positive and negative, respectively. Therefore, it can be seen from Eq. 10 that the two-dimensional plastic shear strain represents the sum of the maximum and minimum principal plastic strains. The two-dimensional plastic shear strain, a variable not only satisfied the three characteristics of the ideal plasticity parameters, but also with a simple form and clear physical meaning, is used by FLAC^{2D} too. So that the correctness of strength parameters (cohesion, the internal friction angle) evolution model of sandstone specimen is convenient to be verified by FLAC^{2D} simulation in the following text.

3.3 Construction of the evolution model of sandstone shear strength parameters

The construction of strength parameter evolution model in this article is based on that the specimen in the yield state (before and after the peak) is satisfied the M-C strength criterion (Comanici and Barsanescu 2016, Martin and Chandler 1994, Wu *et al.* 2018b), and the main steps are as follows, firstly, establish the corresponding relationship between plastic parameters and total stress tensor (strength and confining pressure); then, solve the rock strength parameters under different plastic parameters according to M-C strength criterion and the multiple sets of strength and confining pressure data under the same plasticity parameter; finally, perform curve fitting on the obtained points of discrete strength parameters. Thereby, an evolution model of rock cohesion and internal friction angle can be obtained. What should be noted is that the rock strength mentioned in this paper is the stress extreme value corresponded to the whole process of plastic parameter evolution, but not the peak stress that rock can withstand under a certain confining pressure.

3.3.1 Establishment of the relationship between plasticity parameters and total stress tensor (strength and confining pressure) of sandstone

The cyclic loading and unloading stress-strain curve corresponding to a pressure of 20 MPa is taken as an example to show the building process of the relationship between rock strength and plasticity parameters. It can be


 Fig. 12 Construction method of the relationship between strength (σ_1) and plasticity parameter (σ_p)

 Fig. 13 Relationship between confining pressure σ_3 , strength σ_1 and plastic shear strain γ_p

 Fig. 15 Solution method of cohesion and internal friction angle of sandstone specimen ($\gamma_p=0$)

 Fig. 14 Relationship between rock strength σ_1 and confining pressure σ_3 under the same plasticity parameter γ_p

 Fig. 16 Variation of rock cohesion c and internal friction angle φ with plasticity parameter γ_p

seen from Fig. 11 that there is a unique strain (plasticity parameter) after stress unloading, moreover, the unloading process, with less crack (damage) generated relative to the loading process, influent less on the plasticity parameters (Wang *et al.* 2019). Therefore, the unloading stress σ_u is selected as the maximum principal stress of the rock to establish the relationship between the plastic parameters and the full stress tensor in the yield state of the sandstone specimens. It can be seen from Fig. 12 that at the point of damage stress σ_a , the plastic shear strain of the rock begins to occur (the corresponding $\sigma_{p0} \approx 0$), while the plastic shear

strain is close to 0.07% at the peak stress σ_p . Therefore, the damage stress point should be regarded as the zero point of the plasticity parameter. Through the above analysis, the damage stress is selected as the initial stress of the rock yield state, the relationship between the maximum principal stress / minimum principal stress and plastic shear strain of the sandstone can be constructed by combining with curves in Fig. 8, and the result is shown in Fig. 13. As can be seen from Fig. 13 that under different confining pressures, the maximum principal stresses all increase first, then decrease and finally tend to be stable with the increase of plastic shear strain.

Table 2 Values of rock cohesion and internal friction angle under various plastic parameters

$\gamma_p / \%$	a	b	R^2	c/MPa	$\varphi / ^\circ$
0.00000	68.365	2.763	0.996	20.567	27.931
0.03175	74.308	2.921	0.978	21.740	29.334
0.06349	75.483	2.994	0.969	21.810	29.954
0.09921	75.375	3.114	0.981	21.358	30.919
0.13889	72.685	3.216	0.977	20.265	31.710
0.17857	68.638	3.215	0.967	19.141	31.700
0.23016	63.425	3.167	0.943	17.821	31.333
0.28968	55.596	3.127	0.915	15.719	31.026
0.35714	47.365	3.019	0.886	13.631	30.153
0.44048	36.348	2.952	0.905	10.577	29.603
0.51587	28.388	2.817	0.936	8.458	28.422
0.61111	22.019	2.574	0.950	6.862	26.132
0.71825	17.881	2.377	0.968	5.799	24.064
0.83333	15.534	2.234	0.976	5.197	22.425
0.94841	13.866	2.100	0.982	4.784	20.783
1.06349	12.935	1.989	0.983	4.585	19.327
1.18254	12.009	1.920	0.990	4.334	18.361
1.30556	11.388	1.860	0.995	4.175	17.499
1.42063	10.524	1.844	0.996	3.875	17.268
1.54365	10.184	1.850	0.997	3.744	17.350
1.66667	9.857	1.864	0.996	3.610	17.557
1.78968	9.673	1.858	0.993	3.548	17.472
1.91667	9.645	1.841	0.993	3.554	17.221

3.3.2 Establishment of the relationship between strength and confining pressure under the same plastic strain of sandstone

It can be seen from Fig. 13 that the number of data points obtained by simulation is relatively small, and the sandstone strength corresponding to different confining pressures under the same plastic strain cannot be obtained only by the simulated data points, so the relationship between the rock strength and confining pressure under the same plastic strain is difficult to be established by the discrete data points. However, under different confining pressures, the rock strength changes continuously with the plasticity parameter. Therefore, the trend line of rock strength can be approximately drawn, and then the interpolation method can be applied to obtain the data of rock strength and confining pressure under the same plastic strain, as the elliptic regions shown in Fig. 14. According to the variation of the specimen strength under the yield state with the plasticity parameter, the density of interpolation points gradually become sparse, as shown in Fig. 14.

3.3.3 Solution of cohesion and internal friction angle of sandstone specimen

The M-C strength criterion obtained from Eq. (7) can be expressed by the maximum and minimum principal stresses as follows (Calik and Sadoglu 2014, Zhang *et al.* 2015),

$$\sigma_1 = a\sigma_3 + b \quad (11a)$$

where

$$\begin{cases} a = \frac{1 + \sin \varphi}{1 - \sin \varphi} \\ b = \frac{2c \cos \varphi}{1 - \sin \varphi} \end{cases} \quad (11b)$$

The expression of the internal friction angle and cohesion obtained by the Eq. 11(b) is as follows,

$$\begin{cases} \varphi = \arcsin \frac{a-1}{a+1} \\ c = \frac{b(1-\sin \varphi)}{2 \cos \varphi} \end{cases} \quad (11c)$$

According to the relationship between rock strength and confining pressure under the same plasticity parameter established in Fig. 14, Eq. 11(a) is used for linear fitting to obtain a and b values under the plastic parameter (Zhang *et al.* 2015), and then the corresponding cohesion and internal friction angle can be solved according to Eq. 11(c), as shown in Fig. 15. It can be seen from Fig. 15 that the cohesion and the internal friction angle are 20.567 MPa and 27.931° with the plastic strain being zero. Similarly, the values of cohesion and internal friction angle corresponding to other plastic parameters can be obtained, as shown in Table 2.

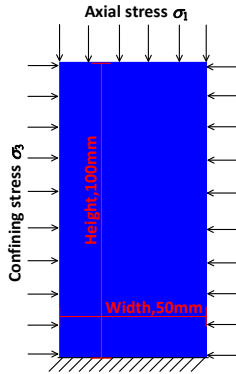
The variation of sandstone cohesion and internal friction angle with plasticity parameter can be drawn according to Table 2, that is, the internal friction angle first increases, then reduces and finally remains unchanged with the increase of plastic parameter, while the sandstone cohesion is without obvious increase process compared with the internal friction angle, as can be seen from Fig. 16.

Specifically, the maximum cohesion of sandstone corresponding to plastic shear strain of 0 is about 21.0 MPa; when the plasticity parameter reaches about 1.4%, the cohesion decreases to about 3.8. MPa, and then the cohesion remains unchanged. For the internal friction angle, in the process of the plasticity parameter increasing from 0 to 0.25%, it gradually increases from about 28.0° to a maximum value of about 32.0°, after that it gradually decreases until the plasticity parameter reaches 1.4%, then the internal friction angle remains about 17.5°. It can be seen from Fig. 14 that the plastic shear strain corresponding to the peak stress, increased with the confining pressure, is about 0.09% under the confining pressure of 20 MPa. Therefore, it is known that the rock cohesion has been reduced to some extent, while the internal friction angle is still rising at the peak stress point according to Fig. 16.

4. Discussion

4.1 Correctness of strength parameter evolution of sandstone

The above describes a method for obtaining the change of cohesion and internal friction angle in the yield state through the cyclic loading and unloading curve of

Fig. 17 FLAC^{2D} model and its boundary conditionsTable 3 Physical and mechanical parameters of FLAC^{2D} model

Parameters	Value
Density ρ / kg/m ³	2700
Yang's modulus E / GPa	32
Poisson's ratio μ^*	0.375, 0.346, 0.301, 0.294, 0.289

*The corresponding confining pressures are 3.5 MPa, 5 MPa, 10 MPa, 15 MPa and 20 MPa, respectively

sandstone, and the mesoscopic mechanism of parameters is also studied. However, that whether the variation of strength parameters is correct needs to be verified. Considering that the two-dimensional plastic shear strain is used as the internal variable of macroscopic strength parameter variation by the strain softening model built in FLAC^{2D} (already mentioned in the section 3.2), the evolution of sandstone cohesion and internal friction angle obtained by the above can be introduced into FLAC^{2D} for confirmatory simulation.

4.1.1 FLAC^{2D} numerical model, constraints and model parameters

The size and boundary constraints of the model are shown in Fig. 17. The model dimensions and boundary conditions are exactly the same as the PFC^{2D} model (see Fig. 5), and the number of elements contained is 20,000. For the model parameters, the change of the rock cohesion and internal friction angle with the plasticity parameters obtained above is introduced into FLAC^{2D} using fish language. The model density is the same as the density of PFC^{2D} particle aggregate (see table 1). The Yang's modulus and Poisson's ratio are determined according to the stress-strain curves obtained by PFC^{2D} simulation (see Fig. 8).

4.1.2 Comparison and analysis between FLAC^{2D} and PFC^{2D} simulation results

The comparison between FLAC^{2D} and PFC^{2D} simulation results is shown in Fig. 18. It can be seen that the stress-strain curves and failure modes (shear failure) obtained by FLAC^{2D} and PFC^{2D} simulation are relatively consistent under various confining pressures, which basically indicates that the two-dimensional plastic shear strain selected in this paper is reasonable as the plasticity parameter, and the

obtained evolutions cohesion and internal friction angle can reflect the stress and deformation characteristics of sandstone.

It is found that under each confining pressure, the stress-strain curves obtained by FLAC^{2D} simulation all agreed well with the PFC^{2D} simulation curves in the pre-peak stage, nevertheless there is a certain error in the softening stage and the residual stage. Specifically, in the softening stage, all the FLAC^{2D} simulation curves are with the obvious phenomenon of stress drop under various confining pressures, while in the residual deformation stage, the FLAC^{2D} simulated stress is higher under low confining pressure than the PFC^{2D} simulation result, and the FLAC^{2D} simulated strain corresponding to the specimen reaching the residual deformation stage under each confining pressure is smaller.

Combined with the failure modes of PFC^{2D} and FLAC^{2D} models under different confining pressures, rock damage simulated by PFC^{2D} is relatively uniform, for there is more than one shear plane. While the softening deformation of FLAC^{2D} model is uneven inside the rock and the strain localization is very obvious. The reason is that the parameter assignment object is each element used as the smallest geometric calculation area in the FLAC^{2D} model, so each element is followed the given strain softening path obtained according to the overall mechanical response of the PFC^{2D} model. In the post-peak stage, a certain strain softening of the elements at the shear plane results in a decrease of the strength parameters, which in turn accelerates the weakening of the elements, so the change of axial stress of the specimen is dominated by the element at the shear plane. The above can be adopted to explain that the FLAC^{2D} model is with a higher stress drop rate in the softening stage and the strain corresponding to the specimen reaching the residual deformation stage is relatively smaller. FLAC^{2D}, a finite difference software, cannot be used to simulate the separation of rock mass after rock failure, however, the dilatancy behavior of rock is more obvious under the lower the confining pressure, as can be seen the Poisson's ratio in table 3. Which may be the reason why the residual stress of FLAC^{2D} simulation under low confining pressure is relatively large.

4.2 Mesoscopic mechanism of the evolution of sandstone cohesion and internal friction angle

For the mesoscopic mechanism of the evolution of sandstone cohesion and internal friction angle, the specimen with the confining pressure of 20 MPa is taken as an example for analysis. Fig. 19(a) and Fig. 19(b) show the corresponding rock crack distribution (shown by the outline of the crack curve) and strength parameter evolution when loaded into different stress states under the confining pressure of 20 MPa. (The points c, d, e, and f in Fig. 19(b) respectively represent the plastic shear strain corresponding to the stress points C, D, E, and F in Fig. 19(a))

(1) O-A stage: In this stage, the bond between the particles cannot be broken due to the relatively small external load. So that there is no crack inside the rock, and the rock cohesion and internal friction angle are mobilized less. The so-called mobilization of rock strength parameters

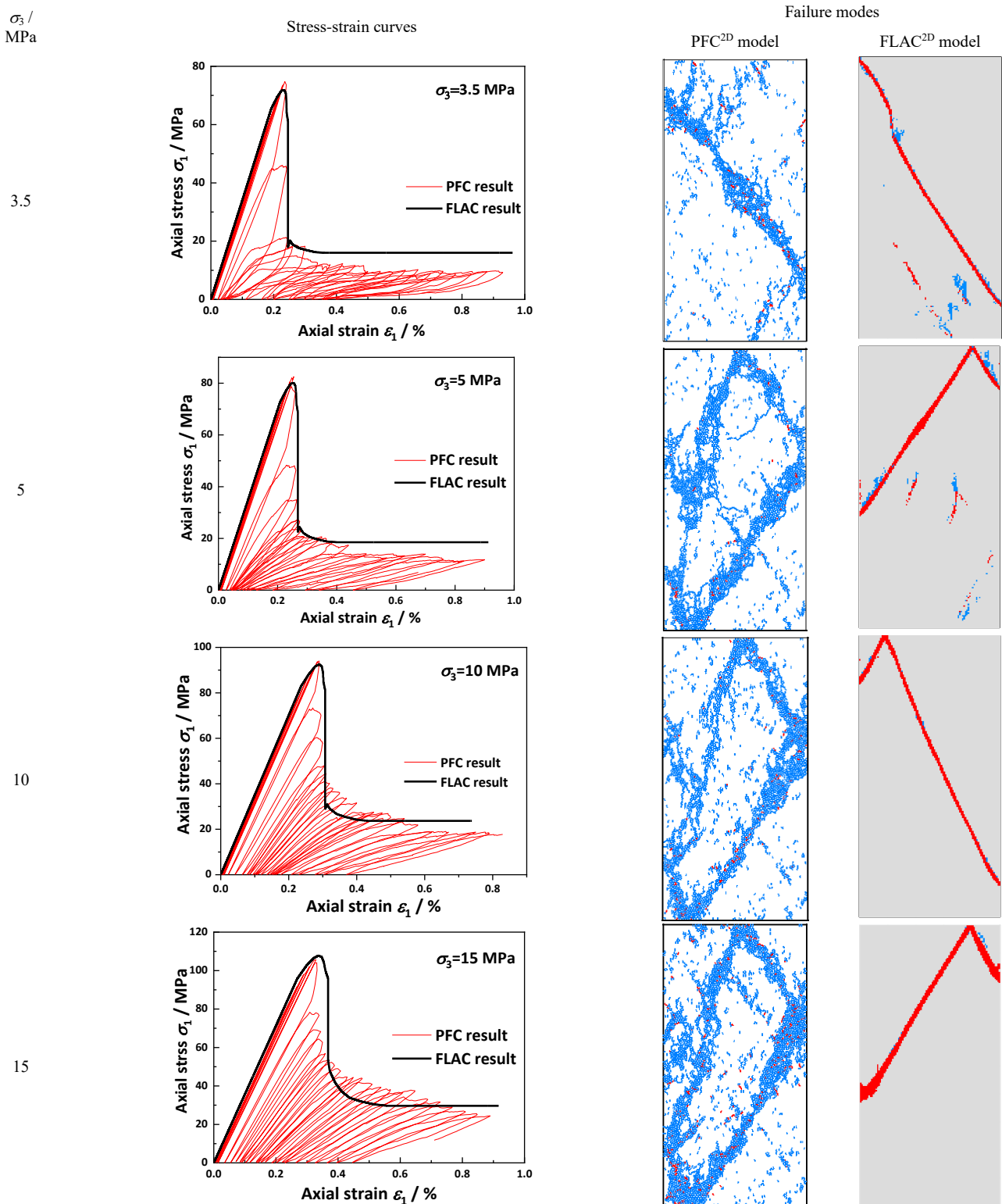


Fig. 18 Comparison between FLAC and PFC simulation results
 Shear cracks (PFC^{2D}) and shear yielded zones (FLAC^{2D}) are indicated by red, while tensile cracks and tensile yielded zones are indicated by blue. It can be seen that the number of tensile cracks in the failure mode adopted by PFC^{2D} simulation is much larger than that of shear cracks, while the shear yielding elements obtained by FLAC^{2D} simulation is much more than the tensile yielding elements. The reason for this difference is that the final failure figure of the PFC^{2D} model indicates all cracks generated during the full loading process of the specimen, while the final failure figure of the FLAC^{2D} model indicates yield states of the element in real-time, which may be completely different from the yield state of the elements in the early loading stage, so the final failure modes of the specimens simulated by the PFC^{2D} and FLAC^{2D} in Fig. 18 are not contradictory.

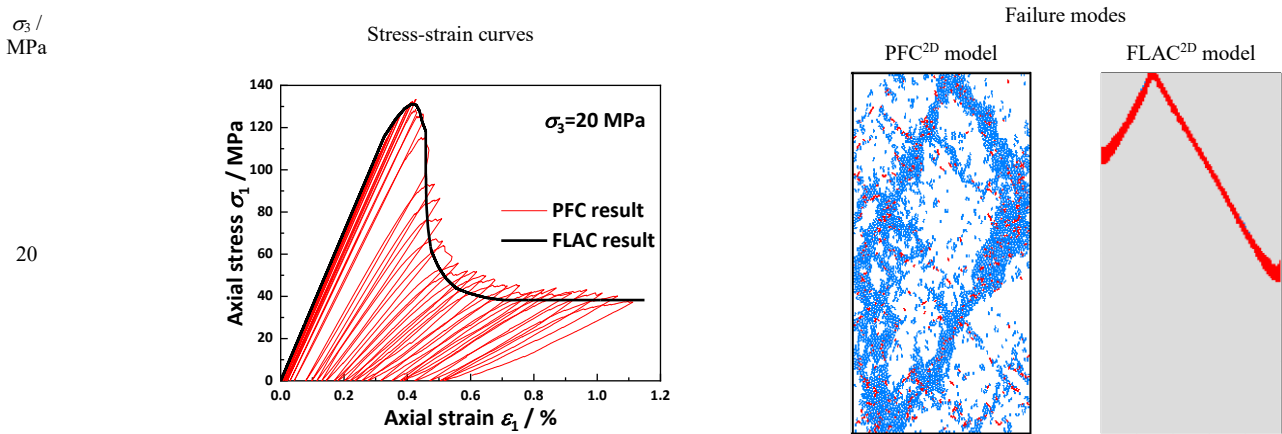
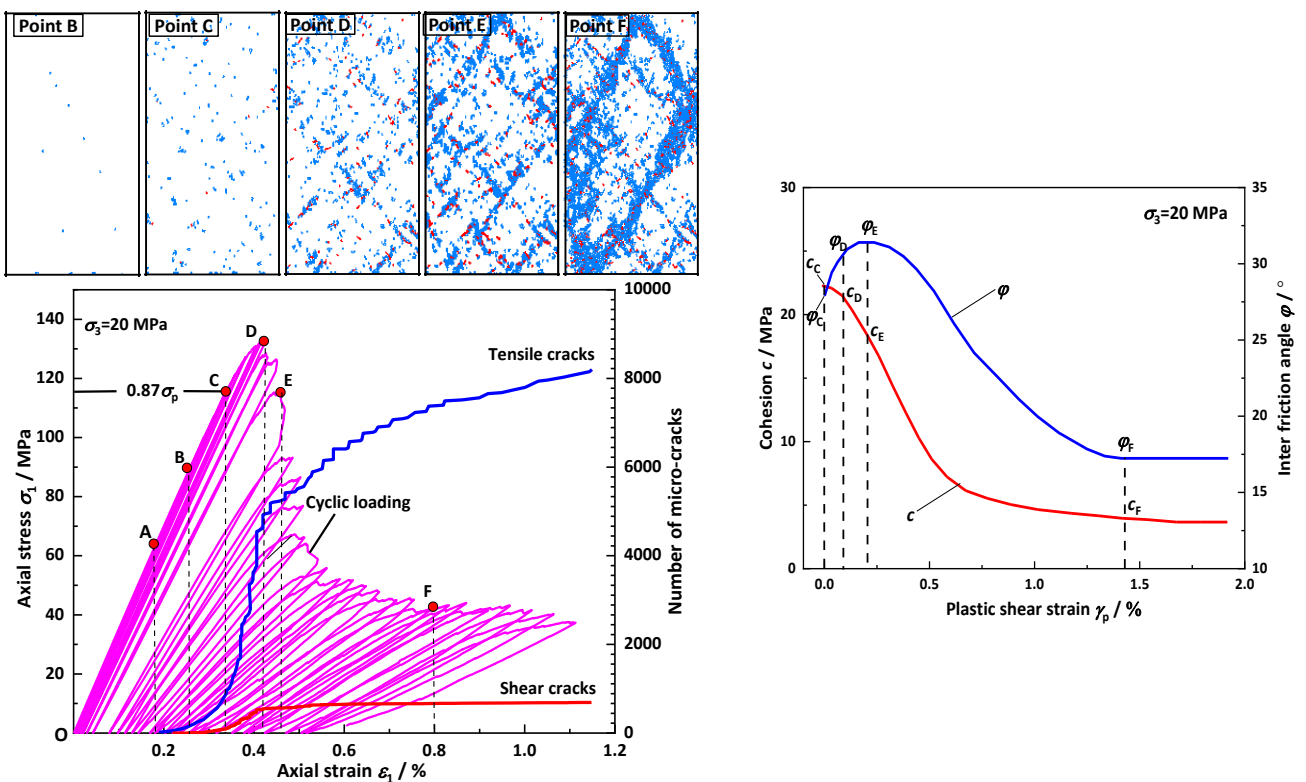


Fig. 18 Continued



(a) Distribution of rock cracks at different loading stages (tensile crack is blue; shear crack is red) (b) Variation of rock cohesion and internal friction angle with plasticity parameter

Fig. 19 Crack propagation and strength parameter evolution during the loading process of sandstone specimen

means that under the effect of the external load, the internal microstructure of the rock will be adjusted accordingly, and the bond and the internal friction between the particles gradually will be mechanical replied to the external load. For example, when there is no load applied on the specimen, the value of strength parameters mobilized is considered as zero.

(2) A-B stage: As the compressive load increases, tensile stress is locally generated in the model. Due to the fact that the bonding state between the particles at different positions inside the specimen is different, which corresponds to the mechanical properties difference of the mineral particles inside the actual rock material, the tensile crack is first

caused at positions where the tensile strength is small. In this stage, the damage of the specimen is small, and the rock cohesion and internal friction angle are not fully mobilized.

(3) B-C stage: In this stage, shear crack inside the specimen begins to occur due to the gradual increase of deviatoric stress, but the micro-damage is still dominated by tensile cracks, as shown in Fig. 19(a). There is approximately only linear elastic deformation occurred inside the specimen before the point C, and the corresponding minor damage (tensile and shear) inside the specimen is randomly and dispersedly distributed, as can be seen the crack distribution corresponding to the point C in

Fig. 19(a). Thus, the plasticity parameter is small or almost zero (point c, see Fig. 19(b)). It can be known from the above definition of rock strength parameter mobilization that sandstone strength parameter mobilized is gradually increasing in the O-C stage. When the damage stress point exceeds point C, the plastic deformation is produced inside the initial yielded specimen, which indicates that the damage of the microstructure inside the specimen can no longer be neglected and the bonds between many adjacent particles are near to destruction, so the rock cohesion is fully mobilized for the first time at point C.

(4) C-D stage: In this stage, 0.091% plastic shear strain is produced corresponding to 0.084% axial strain, as can be seen Fig. 19a and Fig. 19(b). The micro-destruction of the rock begins to increase rapidly and gradually accumulate to be nucleation-cracks with the process of cracks changing the distributed form from randomization to localization and the multi-type cracks interacting with each other (Sun *et al.* 2017, Zhang *et al.* 2015), as the crack distribution corresponding to point D in Fig. 19(a). Which causes the continuity of the specimen to be damaged, so the cohesion is correspondingly reduced (see Fig. 19(b), from point c_C to point c_D). But the interlock effect inside the specimen is created by the interaction of the cracks, which allows the friction angle to be more fully mobilized (from point φ_C to point φ_D , see Fig. 19(b)).

(5) D-E stage: In this softening stage, the damage degree of specimen increases significantly, which is manifested as sharp growth of cracks, connection between nucleated cracks, gradual development of potential slip surface, and significant increase of plastic shear strain (0.112 % plastic shear strain produced corresponding to 0.040 % axial strain, see Fig. 19(a) and Fig. 19(b)), so the cohesion of the rock decreases further (from point c_D to point c_E , see Fig. 19b). But the specimen can still be regarded as a continuous medium with visible cracks. The addition and gradual increased destruction of the interlock resistance inside the specimen occur simultaneously, which is the reason for that the internal friction angle increases by a decreasing rate (from point φ_D to point φ_E , see Fig. 19b).

(6) E-F stage: In this stage, the plastic shear strain and the axial strain increases by 1.217% and 0.341%, respectively, which is accompanied with the gradual formation of shear plane and stress drop of the specimen (Zhang *et al.* 2013). The rock is gradually transformed from the overall load bearing to the common bearing of multiple blocks, as can be seen the rock failure mode corresponding to point F in Fig. 19(a). Correspondingly, the cohesion is continuously reduced to a certain residual value (from point c_E to point c_F , see Fig. 19(b)), and the interlock effect inside the rock is also destroyed by the formation of the sliding shear plane, which causes the internal friction angle to gradually decrease until reached to a residual value (from point φ_E to point φ_F , see Fig. 19(b)).

(7) F- stage: The specimen is in the residual deformation stage, and the external loads is carried by multiple rock blocks. Owing to that the rock deformation mainly slips along the formed shear plane, no much damage happens in rock blocks (Zhang *et al.* 2015). The axial stress, the cohesion and the internal friction angle all remain basically the same at this stage.

5. Conclusions

Plastic shear strain is taken as an internal variable to establish the evolution model of sandstone cohesion and internal friction angle by cyclic loading and unloading simulation tests. The mesoscopic mechanism of the evolution of strength parameters is obtained by combining with the propagation process of micro cracks.

- With the increase of plastic shear strain, the sandstone cohesion first decreases and then tends to be stable, while the internal friction angle first increases, then decreases and finally remains unchanged.
- When the specimen reaches the peak strength, the sandstone cohesion has been reduced to some extent, while the internal friction angle is still rising.
- The evolution of sandstone shear strength parameters is closely related to the whole process of crack formation, propagation and coalescence. As the directional development of the internal micro-fractures as well as the gradual formation of macroscopic shear plane, the rock cohesion reduces continuously and the internal friction angle is in the rise stage. As the formation of the macroscopic shear plane, both the rock cohesion and internal friction angle continuously decrease to a certain residual level.

Acknowledgments

Financial supports for this work, provided by the Fundamental Research Funds for the Central Universities (No. 2018ZDPY08), the National Natural Science Foundation of China (No. 41974164) and the Chinese Government Scholarships (No. 201906420030), are gratefully acknowledged.

References

- Calik, U. and Sadoglu, E. (2014), "Classification, shear strength, and durability of expansive clayey soil stabilized with lime and perlite", *Nat. Hazards*, **71**(3), 1305-1305. <https://doi.org/10.1007/s11069-014-1033-7>.
- Carpenter, B.M., Marone, C. and Saffer, D.M. (2011), "Weakness of the San Andreas Fault revealed by samples from the active fault zone", *Nat. Geos.*, **4**(4), 251-254. <https://doi.org/10.1038/NGEO1089>.
- Castro-Filgueira, U., Alejano, L.R., Arzúa, J. and Ivars, D.M. (2017), "Sensitivity analysis of the micro-parameters used in a PFC analysis towards the mechanical properties of rocks", *Procedia. Eng.*, **191**, 488-495. <https://doi.org/10.1016/j.proeng.2017.05.208>.
- Comanici, A.M. and Barsanescu, P.D. (2016), "Considerations on elliptical failure envelope associated to Mohr-Coulomb criterion", *IOP Conf. Ser. Mater. Sci. Eng.*, **145**(4), 042006. <https://doi.org/10.1088/1757-899X/145/4/042006>.
- Edelbro, C. (2009), "Numerical modelling of observed fallouts in hard rock masses using an instantaneous Cohesion-softening Friction-hardening model", *Tunn. Undergr. Sp. Technol.*, **24**(4), 398-409. <https://doi.org/10.1016/j.tust.2008.11.004>.
- Edelbro, C. (2010), "Different approaches for simulating brittle

- failure in two hard rock mass cases: A parametric study”, *Rock Mech. Rock Eng.*, **43**(2), 151-165.
<https://doi.org/10.1007/s00603-008-0025-x>.
- Haeberli, W., Noetzli, J., Arenson, L., Delaloye, R., Gartner-Roer, I. and Gruber, S. (2010), “Mountain permafrost: development and challenges of a young research field”, *J. Glaciol.*, **56**(200), 1043-1058. <https://doi.org/10.3189/002214311796406121>.
- Hajiabdolmajid, V., Kaiser, P. and Martin, C.D. (2003), “Mobilized strength components in brittle failure of rock”, *Géotechnique*, **53**(3), 327-336. <https://doi.org/10.1680/geot.53.3.327.37280>.
- Joseph, T.G. (2000), “Estimation of the post-failure stiffness of rock”, Ph.D. Dissertation, University of Alberta, Alberta, Canada.
- Langford, J.C. and Diederichs, M.S. (2015), “Reliable support design for excavations in brittle rock using a global response surface method”, *Rock Mech. Rock Eng.*, **48**(2), 669-689. <https://doi.org/10.1007/s00603-014-0567-z>.
- Li, P.F., Zhao, X.G., Guo, Z., Ma, L.K., Chen, L. and Wang, J. (2017), “Variation of strength parameters of Beishan granite under triaxial compression”, *Chin. J. Rock Mech. Eng.*, **36**(7), 1599-1610. <https://doi.org/10.13722/j.cnki.jrme.2016.1412> (in Chinese).
- Martin, C.D. and Changler, N.A. (1994), “The progressive fracture of Lac du Bonnet granite”, *Int. J. Rock Mech. Min. Sci. Geomech. Abstr.*, **31**(6), 643-659. [https://doi.org/10.1016/0148-9062\(94\)90005-1](https://doi.org/10.1016/0148-9062(94)90005-1)
- Qin, Z., Fu, H. and Chen, X. (2019), “A study on altered granite meso-damage mechanisms due to water invasion-water loss cycles”, *Environ. Earth Sci.*, **78**(14), 428. <https://doi.org/10.1007/s12665-019-8426-6>.
- Rafiei, H.R. and Martin, C.D. (2018), “Cohesion degradation and friction mobilization in brittle failure of rocks”, *Int. J. Rock Mech. Min. Sci.*, **106**, 1-13. <https://doi.org/10.1016/j.ijrmms.2018.04.003>.
- Shan, P.F. and Lai, X.P. (2019), “Mesoscopic structure PFC similar to 2D model of soil rock mixture based on digital image”, *J. Vis. Commun. Image R.*, **58**, 407-415. <https://doi.org/10.1016/j.jvcir.2018.12.015>.
- Shi, H., Song L., Zhang, H.Q., Xue, K.K., Yuan, G.T., Wang, Z.S. and Wang, G.Z. (2019a), “Numerical study on mechanical and failure properties of sandstone based on the power-law distribution of pre-crack length”, *Geotech. Eng.*, **19**(5), 421-434. <https://doi.org/10.12989/gae.2019.19.5.421>.
- Shi, H., Zhang, H.Q., Song, L. and Wu, Y. (2019b), “Variation of strata pressure and axial bolt load at a coal mine face under the effect of a fault”, *Arch. Min. Sci.*, **64**(2), 351-374. <https://doi.org/10.24425/ams.2019.128688>.
- Sun, C., Cao, S. and Li, Y. (2017), “Mesomechanics coal experiment and an elastic-brittle damage model based on texture features”, *Int. J. Min. Sci. Technol.*, **28**(04), 639-647. <https://doi.org/10.1016/j.ijmst.2017.11.003>.
- Wang, J., Li, S.C., Li, L.P., Lin, P., Xu, Z.H. and Gao, C.L. (2019), “Attribute recognition model for risk assessment of water inrush”, *Bull. Eng. Geol. Environ.*, **78**(2), 1057-1071. <https://doi.org/10.1007/s10064-017-1159-4>
- Wang, X. and Tian, L.G. (2018), “Mechanical and crack evolution characteristics of coal-rock under different fracture-hole conditions: a numerical study based on particle flow code”, *Environ. Earth Sci.*, **77**(8), 297. <https://doi.org/10.1007/s12665-018-7486-3>.
- Wu, J.Y., Feng, M.M., Mao, X.B., Xu, J.M., Zhang, W.L., Ni, X.Y. and Han, G.S. (2018b) “Particle size distribution of aggregate effects on mechanical and structural properties of cemented rockfill: Experiments and modeling”, *Constr. Build. Mater.*, **193**, 295-311. <https://doi.org/10.1016/j.conbuildmat.2018.10.208>.
- Wu, J.Y., Feng, M.M., Yu, B.Y. and Han, G.S. (2018a), “The length of pre-existing fissures effects on the mechanical properties of cracked red sandstone and strength design in engineering”, *Ultrasonics*, **82**(1), 188-199. <https://doi.org/10.1016/j.ultras.2017.08.010>.
- Zhang, F., Sheng, Q., Zhu, Z.Q. and Zhang, Y.H. (2008), “Study on post-peak mechanical behavior and strain-softening model of Three Gorges granite”, *Chin. J. Rock Mech. Eng.*, **27** (Supp.1), 2 651–2 655. [https://doi.org/1000-6915\(2008\)supp1-2651-05](https://doi.org/1000-6915(2008)supp1-2651-05) (in Chinese).
- Zhang, H.Q., Nunoo, S., Tannant, D.D. and Wang, S.Y. (2015), “Numerical study of the evolution of cohesion and internal friction in rock during the pre-peak deformation process”, *Arab. J. Geosci.*, **8**(6), 3501-3513. <https://doi.org/10.1007/s12517-014-1508-6>.
- Zhang, P., Li, N., Li, X.B. and Nordlund, E. (2009), “Compressive failure model for brittle rocks by shear faulting and its evolution of strength components”, *Int. J. Rock Mech. Min. Sci.*, **46**(5), 830-841. <https://doi.org/10.1016/j.ijrmms.2009.01.002>.
- Zhang, R., Jiang, Z., Sun, Q. and Zhu, S. (2013) “The relationship between the deformation mechanism and permeability on brittle rock”, *Nat. Hazards*, **66**(2), 1179-1187. <https://doi.org/10.1007/s11069-012-0543-4>

CC